

## Session III

Tuesday, September 6 - morning

I3

**WHOLE POWDER PATTERN MODELLING OF NANOCRYSTALLINE AND PLASTICALLY DEFORMED MATERIALS “HANAVALT AWARD LECTURE”****Paolo Scardi**

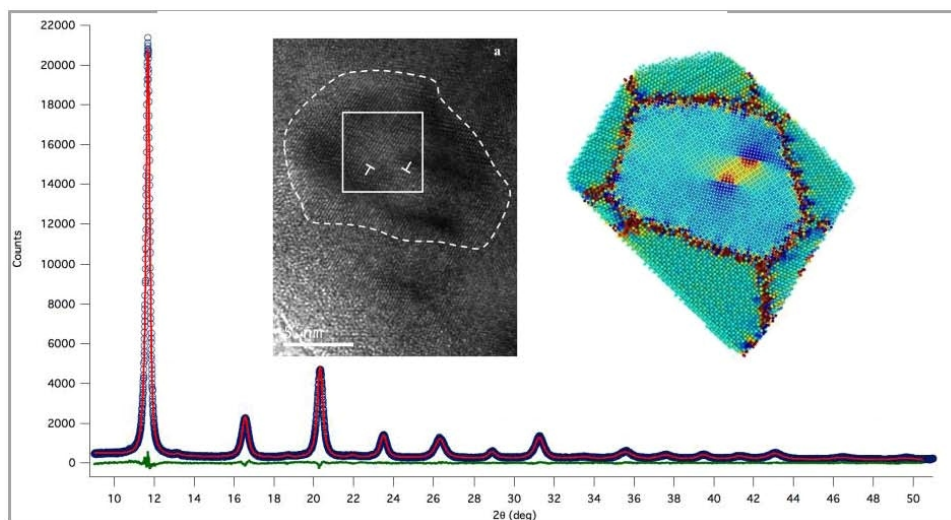
*Department of Civil, Environmental & Mechanical Engineering, University of Trento, Via Mesiano 77,  
38123 Trento, Italy  
Paolo.Scardi@unitn.it*

Whole Powder Pattern Modelling (WPPM) has been extensively used for nearly two decades in the characterization of nanocrystalline and plastically deformed materials, to gather information on crystalline domain shape and size distribution, and on the nature and amount of lattice defects, with special interest to those generating inhomogeneous strain fields [1,2]. In time the WPPM approach has been completed by a variety of microstructural models, with due consideration of diffuse scattering from static and dynamic disorder (Temperature Diffuse Scattering, TDS). The present talk reviews basic theory and applications, introducing the latest WPPM algorithm, adopted by the x-Dream software. Substantial improvements include structural models, as in Rietveld refinement, which add to the microstructural ones; detailed information on results and progress of the WPPM procedure are made visible directly in the user interface.

Among the latest results which will be presented, the growing integration between atomistic modelling, mostly based on Molecular Dynamics simulations, and WPPM. This combination is especially useful to understand how lattice defects – most remarkably, line defects and grain

boundaries – contribute to the inhomogeneous strain and consequent line profile effects [2,3]. More results are presented on powders made of free-standing nanocrystals, as commonly produced and used in modern nanotechnology, e.g., for catalysis and biomedical applications.

1. P. Scardi, in *Powder Diffraction: Theory and Practice* (The Royal Chemistry Society, Cambridge, 2008), edited by R.E. Dinnebier & S.J.L. Billinge. Chap. 13, pp. 376–413. ISBN-13: 978-0854042319.
2. P. Scardi, A. Leonardi, L. Gelisio, M. R. Suchomel, B. T. Sneed, M. K. Sheehan & C.-K. Tsung, “Anisotropic atom displacement in Pd nanocubes resolved by molecular dynamics simulations supported by x-ray diffraction imaging”, *Phys. Rev. B* 91 (2015) 155414. doi: 10.1103/PhysRevB.91.155414.
3. L. Rebuffi, A. Troian, R. Ciancio, E. Carlino, A. Amimi, A. Leonardi & P. Scardi, “On the reliability of powder diffraction Line Profile Analysis of plastically deformed nanocrystalline systems”, *Scientific Reports* 6 (2016) 20712. doi: 10.1038/srep20712.





C7

## TOWARDS REAL TIME X-RAY IMAGING OF CRACKS AND FRACTURE IN SILICON

A. N. Danilewsky<sup>1</sup>, A. Rack<sup>2</sup> and M. Scheel<sup>3</sup>

<sup>1</sup>Kristallographie, Albert-Ludwigs-Universität, 79104 Freiburg i. Br., Germany

<sup>2</sup>European Synchrotron Radiation Facility, Grenoble, France

<sup>3</sup>Synchrotron Soleil, Gif sur Yvette, France

a.danilewsky@krist.uni-freiburg.de

Frank-Read sources in Si as well as thermal slip move in a ductile regime of the crystals at a speed in the order of magnitude of  $10^{-5} - 10^{-6}$  m/s. In X-ray diffraction imaging, effects with a speed up to about  $10^{-3}$  m/s are easily accessible [1]. In the brittle regime, the same driving forces may result in fracture of a crystal with a crack tip speed up to 3600 m/s where the experimental observation in real time becomes a challenge. In this paper we will demonstrate, how the time structure of a brilliant synchrotron light source like ESRF, Grenoble, France can be used to follow ultra high speed events towards a time scale of less than microseconds [2]. In the so called four-bunch mode, only four highly populated electron bunches are used in the storage ring, separated from each other by a temporal delay of around 700 ns. The highest crack tip speed of 70 m/s is recently measured with a high-speed CMOS-based camera system providing frame rates of about 355.000 frames/sec. Based on a frame-transfer CMOS concept, such detector can operate at frame rates of up to 10 000 000 images per second: with a pixel size of about  $40 \mu\text{m}$  it would allow one to follow cracks in real time up to a speed of 2000 m/s.

The experiments presented in this paper are performed on (001) oriented Si slices with artificial starting defects, done with an indentation method. At about  $1100^\circ\text{C}$ , the slices are quenched by a water jet to produce enough thermal stress for crack formation and propagation. With 2 fast camera systems and acquisition rates of about 35 500 images per second the direct and diffracted image of a crack can be followed in parallel. Fig. 1 shows the starting indent

in frame 210 and the appearance of the first crack c1 between frame 308 - 311, covering  $84 \mu\text{s}$ . Information about the geometry and speed of a crack can be taken from the direct image from phase contrast, whereas the related local strain variation becomes visible in the 220 reflection. In this way and within about 42 ms a complex crack pattern of five cracks c1 - c5 originates from the indent, as shown in Fig. 2, frame 1495. Until frame 3000 the cracks elongate with varying strain fields and various crack tip velocities. Careful analysis indicates, that the deflection of the crack face into various high indexed, (hkl) planes is correlated with the short arrests of some microseconds of the crack tip. Obviously the local pile up of energy during the arrest allows to open the higher energy (hkl) faces. An irregular fracture results instead of a mirror like cleavage along the preferred low energy  $\{111\}$  or  $\{110\}$  planes as expected in the diamond structure.

Slow motion movies show this irregular crack propagation directly in phase contrast and in diffraction the related changes in the strain field.

1. A. N. Danilewsky, J. Wittge, A. Hess, A. Croell, A. Rack, T. dos Santos Rolo, D. Allen, P. McNally, P. Vagovic, Z. Li, T. Baumbach, E. Gorostegui-Colinas, J. Garagorri, M. R. Elizalde, D. Jaques, M. Fossati, D. K. Bowen and B. Tanner, Phys. Stat. Sol. (a) 208(11) (2011), 2499-2504.
2. A. Rack, M. Scheel and A. N. Danilewsky, IUCrJ 3(2) (2016), 108-114, DOI: <http://dx.doi.org/10.1107/S205225251502271X>.

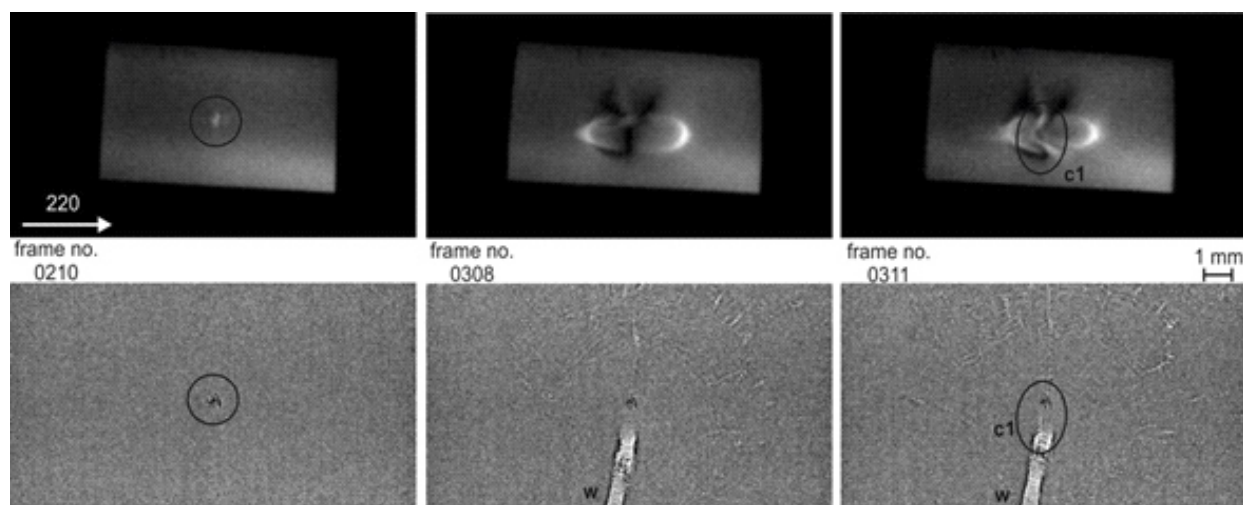


**Figure 1.** Beginning of high speed X-ray imaging of Si (100) wafer at about  $1000^\circ\text{C}$ : (a) 220 Reflection (b) Radiography (phase contrast), both  $1.28 \mu\text{s}$  integration time and  $28 \mu\text{s}$  frame distance: Frame 210: indent marked by circle, Frame 308: locally quenching with a water jet (w) produces a strain field, Frame 311:  $84 \mu\text{s}$  later the first crack c1 modifies the strain field (marked by ellipse).

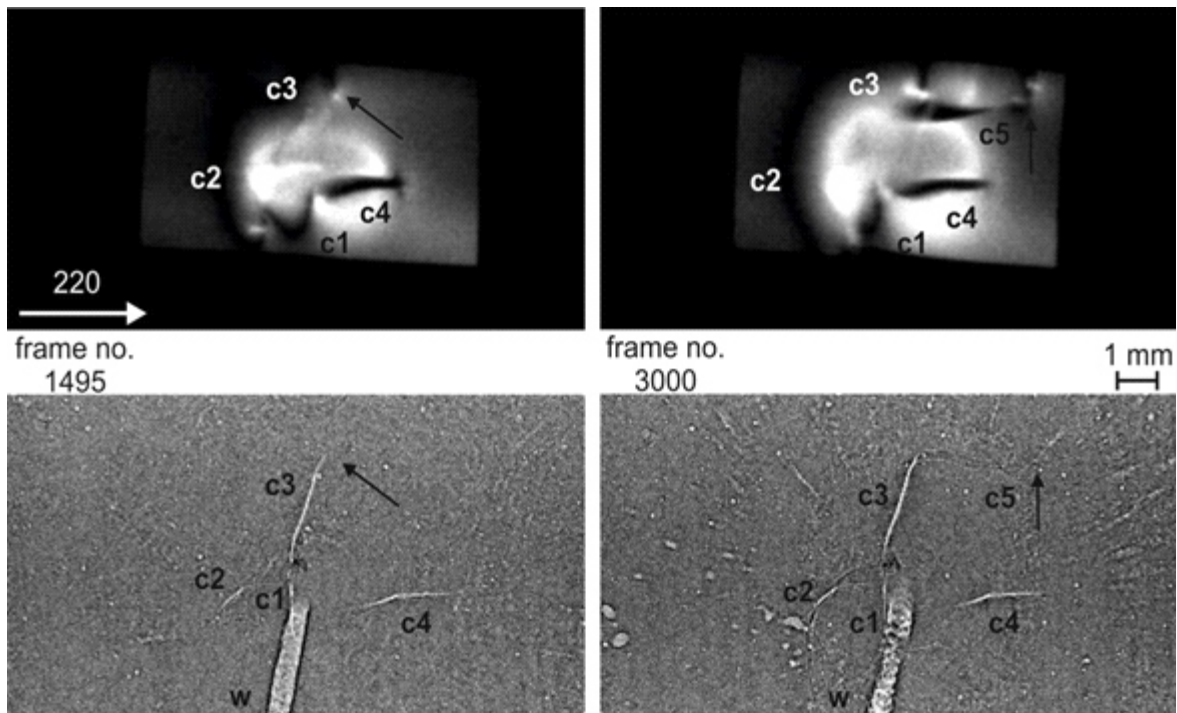


**Figure 2.** Continued high speed X-ray imaging of Si (100) wafer at about 1000 °C from Fig. 1 (a) 220 reflection (b) Radiography (direct image, phase contrast): Frame 1495 after 42 ms: cracks c2, c3, c4 and surrounding strain, arrow indicates tip of crack c3, Frame 3000 after about 0.1 s: last crack c5, tip marked by arrow.

The authors wish to acknowledge Prof. B. Tanner, Dept. of Physics, Durham, UK and Prof. P. McNally School of

Electronic Engineering, Dublin City University, Dublin, Ireland for helpful discussions.

C8

## NON-DESTRUCTIVE X-RAY DIFFRACTION MEASUREMENT OF WARPAGE IN SILICON DIE EMBEDDED IN INTEGRATED CIRCUIT PACKAGES

B. K. Tanner<sup>1</sup>, A. N. Danilewsky<sup>2</sup>, A. Bose<sup>3</sup>, R. K. Vijayaraghavan<sup>3</sup>, A. Cowley<sup>3,4</sup>, V. Cherman<sup>5</sup> and P. J. McNally<sup>3</sup>

<sup>1</sup>Dept. of Physics, Durham University, South Road, Durham DH1 3LE, U.K

<sup>2</sup>Kristallografie, Albert-Ludwigs-Universität, Freiburg, Germany

<sup>3</sup>School of Electronic Engineering, Dublin City University, Dublin 9, Ireland

<sup>4</sup>Currently at European Astronaut Centre, European Space Agency, Köln, Germany

<sup>5</sup>IMEC, Kapeldreef 75, B-3001 Louvain, Belgium.

b.k.tanner@dur.ac.uk

Future integrated chip manufacturing must encompass complex chip systems capable of diverse functionality and application, so-called “More than Moore” manufacturing. Such systems include Micro-Electromechanical Systems, System in Package, System on Chip and 3-D Integrated Circuits, referred to collectively as “advanced packages”. This technology requires processing of thin semiconductor die (25-100 $\mu$ m thickness) and many packages include multiply-stacked silicon die. A recent review [1] revealed that none of today’s commercially available metrology tools is capable of measuring, *in situ* and non-destructively across an entire die, the nature and scale of wafer/die strain or bow/warp. Many techniques are destructive and those that are non-destructive tend to measure the package bow which, crucially, is not the same as wafer/die bow.

We have demonstrated that X-Ray Diffraction Imaging (XRDI) using B-Spline fitting techniques (B-XRDI) is capable of non-destructive, *in situ* mapping and analysis of major die warpage features in fully encapsulated advanced packages [2-3]. We describe how B-XRDI allows the user to reconstruct, from the image distortion of a series of section x-ray topographic images, a full profile of the warpage of the silicon die inside such a chip package. There is no requirement for pre-treatment or pre-processing of the chip package. We have used the technique to demonstrate the impact of elevated temperature on a commercially sourced micro quad flat nonlead (uQFN) chip package and have shown that the strain becomes locked in at a temperature between 94°C and 120°C [4]. Using synchrotron radiation at the Diamond Light Source, warpage maps for the entire 2.2 mm  $\times$  2.4 mm  $\times$  150  $\mu$ m Si die were acquired in 50 s and

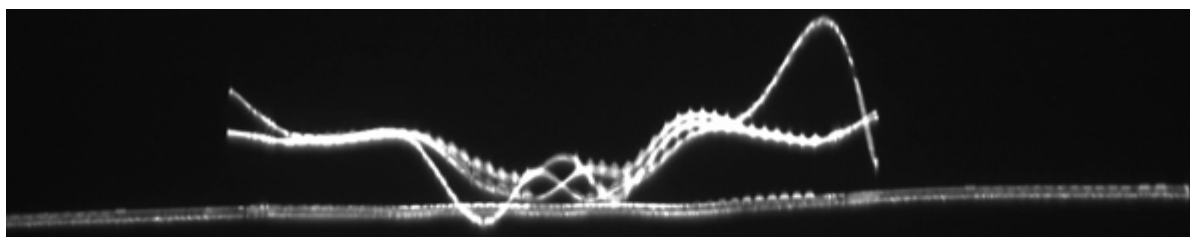


**Figure 1.** White beam section topographs of a package containing 4 stacked Si die. The 3 top dies are 5 mm 5 mm 50  $\mu$ m thick, while the bottom die is 8 mm 8 mm 200  $\mu$ m thick.

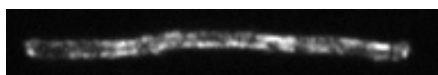


**Figure 2.** Image from a distorted (001) oriented uQFN die taken in transmission with a wide area monochromatic beam.

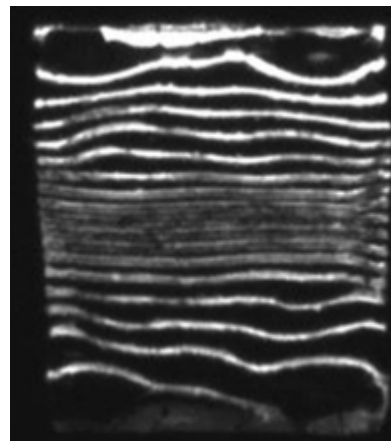


**Figure 3.** Summed monochromatic topographs taken at equal steps across the rocking curve for a packaged uQFN die. Adhesive is applied at the four corners of this die prior to encapsulation. 220 reflection.

individual line scans in 500 ms. Warpage in multiple die packages (Fig1) has been measured.

We present examples of warpage measurement in several commercial chip packages and by measuring the image displacement as a function of detector distance and at several wavelengths, tilt and strain have been determined independently. The data have been shown to be in good agreement with warpage in test structures determined from mechanical profilometry.

Using a monochromatic beam, the warpage data can also be collected by recording transmission X-ray topographs at different angular positions across the rocking curve. Due to the wafer deformation, a narrow stripe of intensity only is imaged for any one angle (Fig 2). Addition of sequential stepped images creates the “zebra pattern” of Renninger [5] and this directly represents contours of effective misorientation. In this mode, strain sensitivity is limited by the X-ray optics. We have shown that statistically good data can be taken in transmission on single chip packages at 24.25keV (Fig 3), close to the wavelength of the AgK line. The total data collection time for the 20 images in Fig 3 was 75 seconds at B16 of the Diamond Light Source. By comparing 220 and reflections, we show that the deformation is almost symmetrical on 90 rotation about the [001] surface normal. Reversal of the entrance and exit surface results in similar patterns but with displacement of successive images in opposite directions. Contour analysis between these settings provides a means of separating tilts and dilations.

We compare the two approaches to warpage measurement in packaged die and examine the possibilities and challenges of converting the techniques into an in-fab tool.

1. M.R. Marks, Z. Hassan, K.Y. Cheong, *IEEE Trans. Comp. Manuf. Technol.*, **4**, (2014) 2042.
2. C.S. Wong, N.S. Bennett, D. Manassis, A. Danilewsky, P.J. McNally, *Microelectronic Engineering* **117** (2014) 48.
3. A. Cowley, A. Ivankovic, C.S. Wong, N.S. Bennett, A.N. Danilewsky, M. Gonzalez, V. Cherman, B. Vandeveld, I. De Wolf, P.J. McNally, *Microelectronics Reliability*, **59**, (2016), 108.
4. A. Bose, R.K. Vijayaraghavan, A. Cowley, V. Cherman, O. Varela Pedreira, B.K. Tanner, A.N. Danilewsky, I. De Wolf, P. J. McNally, *IEEE Trans. Comp. Packag. Manuf. Technol.*, **6** (2016) 653.
5. M. Renninger *Phys Lett* **1** (1962) 106.

## DETERMINABILITY OF DISLOCATION PATHS BY 3D DIFFRACTION LAMINOGRAPHIC IMAGING: THEORETICAL CONSIDERATIONS LEADING TO A NEW EXTINCTION RULE

D. Hänschke<sup>1,2</sup>, T. Baumbach<sup>1,2</sup>

<sup>1</sup>Karlsruhe Institute of Technology (KIT), Institute for Photon Science and Synchrotron Radiation (IPS/ANKA), 76344 Eggenstein-Leopoldshafen, Germany

<sup>2</sup>Karlsruhe Institute of Technology (KIT), Laboratory for Applications of Synchrotron Radiation (LAS), 76128 Karlsruhe, Germany  
daniel.haenschke@kit.edu

Recently, X-ray diffraction laminography (XDL) has been developed and successfully applied to the 3D imaging of dislocation networks inside large monocrystals like e.g. industrial silicon wafers [1]. Similar to X-ray topo-tomography [2] and related electron tomographic approaches [3], XDL is based on the acquisition of topographic (i.e. Bragg diffraction contrast) projection images of the investigated crystal volume during its rotation about a selected reciprocal lattice vector. The average distribution of the local reflectivity (for suitable contrast conditions increased close by crystal defects like dislocations) can then be estimated by means of 3D laminographic reconstruction with suitable algorithms. In many cases, this enables the determination of the spatial dislocation arrangement with few micrometres precision.

It turns out, however, that few dislocation segments with certain configurations of local line direction  $\mathbf{l}$ , Burgers vector  $\mathbf{b}$ , diffracting reciprocal lattice vector  $\mathbf{h}_{\text{hkl}}$ , and direc-

tion  $\mathbf{k}_h$  of the diffracted beam, cannot be localized inside the reconstruction volume in this way. In the simplest case, this is due to the well-known extinction rule for vanishing or reduced topographic contrast of dislocations (basically  $\mathbf{b} \cdot \mathbf{h}_{\text{hkl}} = 0$ ), i.e. the defects are already not sufficiently visible in the entire projection data in the first place. But, more intriguingly, in some cases only the paths of particular dislocation segments cannot be determined, despite these being clearly visible in most projections. Up to now, this effect has not been understood.

We will report on our recent investigation of the X-ray diffraction contrast of dislocations during XDL measurements, using linear elasticity theory [4]. We will show that for projection acquisition with both full excitation (e.g. by white beam) and so-called weak-beam conditions [5] analytic expressions can be derived for the size of the excited crystal volume  $V$  per dislocation line length, in dependence of the projection angle  $\phi$ , see Fig. 1 and Fig. 2. Based on this, we will formulate a new extinction rule, which correctly predicts the inaccessibility of a certain class of dislocation segments. For the future this will allow a more careful interpretation of dislocation arrangements determined by any projection based 3D diffraction imaging.

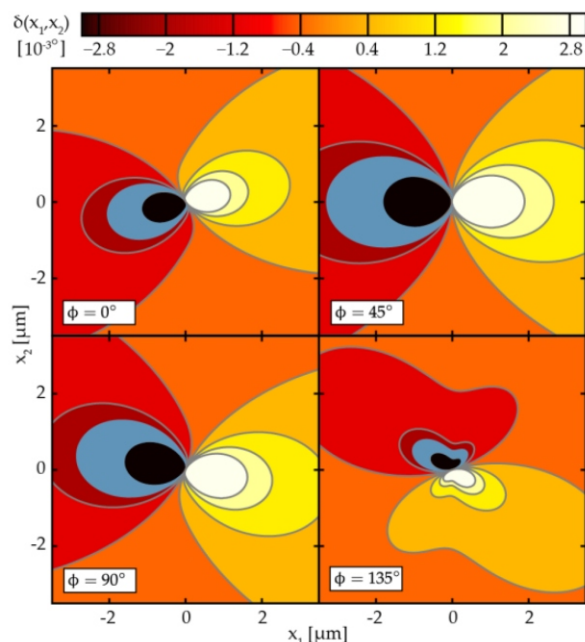


**Figure 1.** Numerical simulation of the effective misorientation  $\delta(x_1, x_2)$  of the diffracting lattice planes close by a dislocation in silicon, for different view angles  $\phi$  during rotation about the reciprocal lattice vector  $\mathbf{h}_{2-20}$ . Line direction is  $\mathbf{l} = \mathbf{e}_3 = [01\bar{1}]$ , the Burgers vector is  $\mathbf{b} = a/2[101]$  and  $E = 40$  keV. The corresponding excited crystal regions  $V$  for a fixed interval  $\Delta\phi$  are indicated as blue areas.

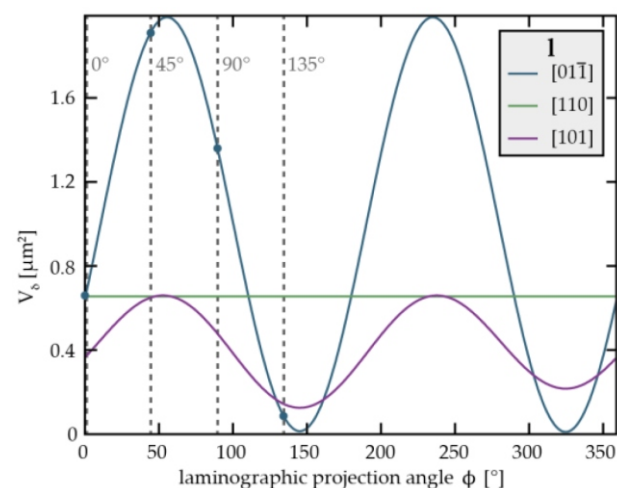


**Figure 2.** Fully analytic calculation of the excited crystal volume per line length  $V$  (fixed  $\Delta\phi$ , the same as for Fig. 1), in dependence of the rotation angle  $\phi$ . Three line directions  $\mathbf{l}$  are compared (blue corresponding to Fig. 1), revealing significant differences. From the underlying analytic expressions an extinction rule can be derived, predicting the failure of dislocation path determination by 3D reconstruction from projections.



1. D. Hänshcke, L. Helfen, V. Altapova, A. Danilewsky, T. Baumbach, *Appl. Phys. Lett.*, **101**, (2012), 244103.
2. W. Ludwig, P. Cloetens, J. Härtwig, J. Baruchel, B. Hamelin, P. Bastie, *J. Appl. Crystallogr.*, **34**, (2001), 602-607.
3. J. S. Barnard, J. Sharp, J. R. Tong, P. A. Midgley, *Science*, **313**, (2006), 319.
4. J. P. Hirth, J. Lothe, *Theory of dislocations*. New York: MacGraw-Hill. 1968.
5. A. Authier, *Dynamical theory of X-ray diffraction*. Oxford: Oxford University Press. 2002.

*The presented work is partially funded by the EU-FP7 project No. 216382 SIDAM and by the German Federal Ministry of Education and Research by the grant 05K14VKA STROBOS-CODE. We thank for the support and valuable contributions by all members of these collaborations as well as by the staff of IPS, LAS, and IBPT/ANKA.*

C10

## COMBINING QUALITATIVE AND QUANTITATIVE DIFFRACTION TOPOGRAPHY AT THE ESRF TO CHARACTERISE PV SILICON AND DIAMOND CRYSTALS

T. N. Tran Thi<sup>1</sup>, V. A. Oliveira<sup>2</sup>, D. Camel<sup>2</sup>, S. Connell<sup>3</sup>, D. Caliste<sup>4</sup>, D. Eon<sup>5</sup>, J. Härtwig<sup>1</sup>, T. Lafford<sup>6</sup>, J. Baruchel<sup>1</sup>

<sup>1</sup>European Synchrotron Radiation Facility (ESRF), BP 220, 38043 Grenoble, France

<sup>2</sup>INES, CEA, Le Bourget du Lac, F-73000, France

<sup>3</sup>University of Johannesburg, Auckland Park, South Africa

<sup>4</sup>L Sim, MEM, UMR-E CEA/UGA, INAC, Grenoble F-38054, France

<sup>5</sup>Institut Néel, CNRS, Grenoble, France

<sup>6</sup>IBEX Innovations Ltd., NETPark, Sedgefield, TS21 3FH, UK

The need for high quality diamonds, for electronics, detectors and X-ray optics purposes, and for “inexpensive, reduced-defects” silicon for photovoltaic (PV) purposes, has strongly promoted the use of X-ray Bragg diffraction imaging (“X-ray topography”) techniques to study their defects. This led us to develop, at the ESRF, enhanced capabilities in the portfolio of Bragg imaging techniques we now propose. This includes some automation, and a new diffractometer on the BM05 beamline. Within this portfolio, projection and section white beam topography and monochromatic Rocking Curve Imaging (RCI) [1] are mostly used to qualitatively and quantitatively characterise the crystalline quality, in deposited layers, deep bulk structures and the interface between them, with an angular precision in the  $\mu\text{rad}$  range and a spatial resolution in the  $\mu\text{m}$  range.

Diamond exhibits many attractive properties for electronic and detector applications (wide band gap, high mobility of charge carriers, high electric field breakdown strength and thermal conductivity). In addition, diamond, because of its thermal and X-ray transparency properties, is a material of choice for diffractive and refractive X-ray optics [2]. High voltage diodes and FET switches are based on Boron- and phosphorus-doped diamond, these devices being expected to efficiently commute high power at high frequency. But their performances are a function of the crystalline quality, and the material available from commercial suppliers covers a wide variety of qualities and prices. Figure 1 shows examples of topographic images made at BM05: the high quality type-IIa diamonds (Fig. 1 iii and vi) display areas of the (001) growth sector that are

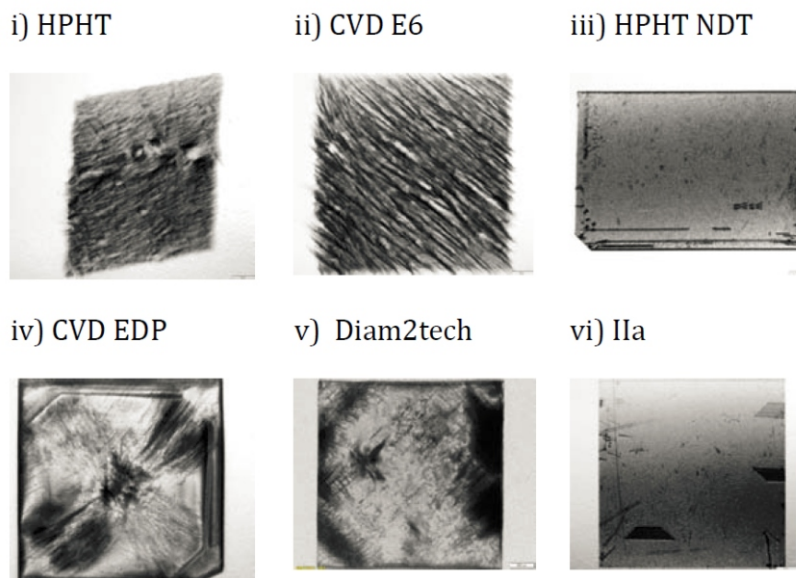


**Figure 1:** White beam topographs of different single diamond plates characterized at BM05

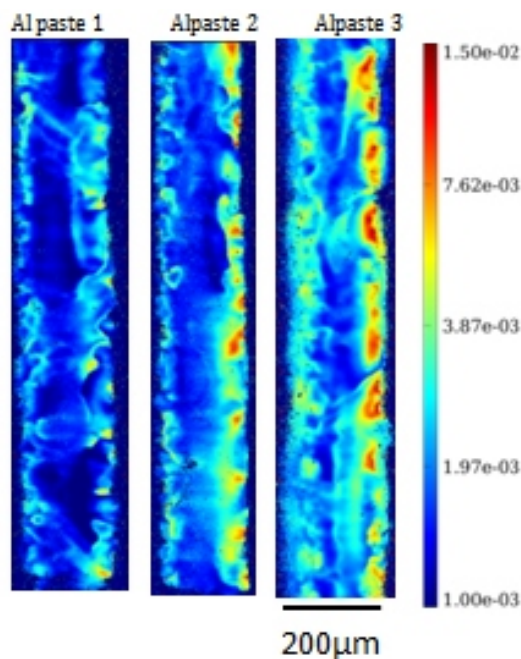


**Figure 2.** 220 section FWHM maps (in degrees) of mono-like Si, with Al back-planes made from three different Al pastes. The face with the Al back plane is on the right of the image. The Al back plane produces an increased distortion of the Si 220 planes, higher than the one associated with the mono-like Si defects formed during the growth (visible within the bulk of the sample). The different Al pastes produce different effects: the Si 220 FWHM values vary significantly when going from the Al paste 1 (“good” photovoltaic efficiency, less distortion of the Si wafer, FWHM values  $\sim 2 \times 10^{-3}$  degrees) to, Al paste 3 (“less good”, FWHM misorientations of the Si wafer up to  $8 \times 10^{-3}$  degree).

almost dislocation-free, with only a few stacking-faults visible. The dislocation densities of ‘low grade’ commercial diamonds (images i, ii, iv and v) are in the  $10^3$ - $10^4 \text{ cm}^{-2}$  range. The crystalline quality of a boron-doped layer grown onto a diamond plate was quantified via section RCI measurements (FWHM maps). It shows that the distortion of the boron-doped layer ( $\text{FWHM} > 3.5 \cdot 10^{-3}$  degrees) is much higher than that of the substrate bulk ( $\text{FWHM} \sim 2.4 \cdot 10^{-3}$  degrees). But attention should also be paid to the defects that exist in the diamond substrate itself (dislocations,

stacking faults, growth sectors, and (sub-) surface damage from polishing processes), these defects being often detrimental for the final electronic performance.

Silicon is today the most widely-used material for PV applications. Both the quality of PV-Si substrates and the preparation of the device, strongly influence the PV efficiency and price of the solar-cell. We have therefore studied both the growth of “mono-like” Si (less expensive than Cz Si, but sufficient quality for PV applications) and aspects of the cell processing (Al back electrical contacts).

The “mono-like” Si is grown by directional solidification, on a series of seeds located at the bottom of the crucible. Dislocation sources, leading to a dislocation multiplication very detrimental for the PV efficiency, occur during growth, both at the level of the junction of the seeds [3] or higher in the ingot through the piling up of dislocations belonging to several gliding systems [4]. These two mechanisms have been widely studied through white beam and RCI measurements.

The distortion and strain of the Si in contact with the Al back layer have been characterised by coupling RCI section topography with X-ray nano-diffraction measurements (at ID01). The results show a correlation between the lattice distortion of the Si in contact with the eutectic and Al layers, and the PV efficiency. This distortion, and the PV performances, vary as a function of the Al paste used. The higher PV efficiency (“good” paste) appears to be associated with a higher homogeneity of the eutectic layer and, consequently, a lower distortion of the Si back surface region (Fig.2). The difference between the various commercial pastes rests on the amount of Al, Al grain size, and their precise composition. We determined some of the characteristics of a “good Al paste”, a crucial ingredient for producing efficient solar cells.

1. R.T. Kluender, A. Philip, J. Meyssonier, J. Baruchel, *Phys. Status Solidi* **208**, 2505 (2011).
2. P. Van Vaerenbergh, C. Detlefs, J. Härtwig, et al., *AIP Conf. Proc.* 1234, 229 (2010).
3. M. Tsoutsouva, V.A. Oliveira, D. Camel, T.N. Tran Thi, et al., *J. Cryst Growth* **401**, 397 (2014).
4. V. Amaral de Oliveira, PhD Thesis, Université Grenoble Alpes (2016).
5. T. N. Tran Thi, S. Dubois, J. Baruchel et al. *Solar Energy Materials and Solar Cells* **135**, 17 (2015).